Antibody Mediated Diversification of Primary and Secondary Immune Responses

Dennis Schaefer-Babajew[1*†], Laurine Binet[1*], Gabriela S. Silva Santos[1], Chiara Ruprecht[1], Lachlan P. Deimel[1], Mohamed A. ElTanbouly[1], Dounia Gharrassi[1], Clara Uhe[1], Kai-Hui Yao[1], Brianna Hernandez[1], Parul Agrawal[2], Anna Gazumyan[1], Leonidas Stamatatos[2], Harald Hartweger[1+], Michel C. Nussenzweig[1,3,+]

[1]Laboratory of Molecular Immunology, Rockefeller University; New York, NY, USA.

[2]Fred Hutchinson Cancer Center, Seattle, WA, USA

[3]Howard Hughes Medical Institute, The Rockefeller University; New York, NY, USA.

[†]Current address: Department of Internal Medicine, Yale School of Medicine, New Haven, CT, USA

*equal contribution

+equal contibution

Address correspondence to: nussen@rockefeller.edu or hhartweger@rockefeller.edu

Summary

Humoral immune responses diversify over time but whether secreted antibodies influence this process is unknown. Using antibody secretion-deficient mice this study shows a profound impact of secreted antibodies on the development of B cell diversity after vaccination.

Abstract

Humoral immune responses are characterized by increasing antibody affinity and diversity over time. Increased affinity is mediated by a combination of immunoglobulin gene somatic mutation and iterative cycles of selection in germinal centers. Less is understood about how diversity increases in parallel with affinity. Here we examine the role of antibody feedback in diversifying immune responses in mice that produce B cells that are incapable of secreting antibodies. To this end, we produced two strains of mice, one that expresses only membrane and secreted forms of IgM, and a second that produces only the membrane bound form of IgM. Analysis of primary and secondary immune responses show that antibody feedback significantly diversifies both primary and secondary immune responses even when antibodies are present at levels that are 10–30 fold lower than physiologic. The data have significant implication for sequential vaccination approaches aimed at shepherding immunity to produce broadly neutralizing antibodies to highly diversified pathogens such as HIV-1 and Influenza.

43 ## Introduction

44 Both the affinity and diversity of antibodies elicited by immunization or infection
45 increase over time by a process that involves iterative cycles of selection, clonal
46 expansion and somatic mutation in germinal centers (GCs) (Bannard and Cyster,
47 2017; Victora and Nussenzweig, 2022).

48

49 These two apparently discordant features of humoral immune responses, increasing
50 affinity and diversity, can be accounted for by dynamic changes in selection over time
51 and by the existence of two cellular compartments, plasma cells and memory B cells
52 respectively. Plasma cells develop by a mechanism that ensures increasing circulating
53 antibody affinity (Zotos and Tarlinton, 2012; Nutt *et al.*, 2015; Tas *et al.*, 2016; Kräutler
54 *et al.*, 2017; Ise and Kurosaki, 2020; ElTanbouly *et al.*, 2024; MacLean *et al.*, 2025).
55 Memory B cells are selected by a separate mechanism that features diversity over
56 affinity (Suan, Sundling and Brink, 2017; Wang *et al.*, 2017; Viant *et al.*, 2020; Inoue
57 *et al.*, 2021; Inoue, Shinnakasu and Kurosaki, 2022).

58

59 Antibody diversification becomes increasingly important during secondary or booster
60 immune responses, when only small numbers of high affinity antigen binding cells can
61 be detected in GCs (Dal Porto *et al.*, 2002; Eckl-Dorna *et al.*, 2019; Mesin *et al.*, 2019;
62 Malladi *et al.*, 2025). Given the strong selection pressure imposed by iterative cycles
63 of mutation and cell division in the GC the evolution away from high affinity is
64 counterintuitive. However, diversification may be an important evolutionary adaptation
65 to deal with rapidly changing pathogens such as Coronaviruses and Influenza virus
66 (Heyman, 2000; Cyster and Wilson, 2024).

Several mechanisms have been suggested to account for the increase in diversity and loss of detectable antigen binding in late primary and secondary GCs. These include: 1. Continual recruitment of additional lower affinity cells during the reaction (De Carvalho *et al.*, 2023; Hägglöf *et al.*, 2023); 2. Increasing T cell fitness that lowers the threshold of B cell selection (Woodruff *et al.*, 2018; Merkenschlager *et al.*, 2023); 3. Antibody mediated antigen masking or enhancement (Heyman, 2000; Cyster and Wilson, 2024).

The effects of antibody feedback on immune responses have been studied since 1909 when they were first described by Theobald Smith in experiments on Diphtheria toxin (Smith, 1909). Recent data shows that masking appears to be mediated by high affinity antibodies and enhancement by low concentrations or low affinity antibodies that may be present even before immunization or in the early stages of the immune response (Heyman, 2000; Cyster and Wilson, 2024). But because all experiments to date, including Smith's, have been performed in organisms that have at least some level of circulating antibody, precisely how masking and enhancement contribute to the evolution of humoral immunity and GC dynamics remains to be determined. Understanding these phenomena is increasingly important in developing strategies for sequential vaccination for difficult pathogens such as malaria parasites, HIV-1 and Influenza virus where antibody mediated masking can interfere with the evolution of immunity in response to serial vaccine boosters.

90 Here we examine the role of antibody feedback in regulating GC responses in mice
91 that have an intact polyclonal B cell compartment but do not secrete antibodies.
92

93 ## Results

94 **Antibody secretion deficient mice**

95 To examine how secreted antibodies impact the development of immune responses
96 we engineered the IgH locus to produce two strains of mice: a control strain that
97 expresses membrane and secreted forms of IgM (M-only) but no other isotypes; and
98 a second strain whose B cells express only the membrane-bound form of IgM (mM-
99 only) (Figure 1A). To this end, the C57BL/6J Ig heavy chain locus was modified using
100 CRISPR-Cas9 to delete a 150 kb region 5' of *Ighd* exon 1 to the 3' UTR of *Igha*, leaving
101 only the IgM locus intact (M-only mice, see methods for further details). M-only mice
102 were subsequently engineered to produce the mM-only mice by removing the stop
103 codon of the secreted splice form and its intronic polyadenylation signal in *Ighm* exon
104 4 (Danner and Leder, 1985; Nussenzweig *et al.*, 1987; Boes *et al.*, 1998; Ehrenstein
105 *et al.*, 1998; Waisman *et al.*, 2007). The later abrogates production of the secreted
106 form by preventing its termination thereby enforcing splicing to produce the
107 membrane-bound isoform of IgM.

108 Consistent with the observation that membrane bound IgM regulates B cell
109 development in the bone marrow (Nussenzweig *et al.*, 1987, 1988; Kitamura *et al.*,
110 1991), M-only and mM-only mice showed generally normal numbers of pro-B, pre-B,
111 immature and mature B cells in the bone marrow (Figure 1B, Supp.Fig.1B-I).
112 Moreover, the numbers of transitional, or mature B2 cells in spleen were similar. As
113 reported by others, mice lacking secreted Igs, show small increases in splenic B1 and

114 marginal zone B cells in the mesenteric lymph nodes but not in Peyer's patches (Figure
115 1C,D Supp.Fig.1E-F). There were few if any plasma cells in the bone marrow of mM-
116 only mice and a decrease that did not reach statistical significance in M-only mice
117 (Figure 1E, Supp.Fig.1A,C,D). Serum ELISAs performed under steady state
118 conditions showed slightly increased IgM but no other isotypes in M-only mice and no
119 detectable antibody in mM-only mice (Figure 1F, Supp.Fig.1A, P=0.0017). Despite the
120 absence of other isotypes, single-cell Ig mRNA sequencing showed that the Ighv, Igkv
121 and Iglv usage by follicular B cells was similar in wild type (WT), M-only and mM-only
122 mice (Figure 1G, Supp.Fig.1H). In summary, B cell development appears largely
123 normal, but in the absence of antibody secretion there are no serum antibodies and
124 few if any plasma cells in mM-only mice.
125
126 **Primary immune responses**
127 To determine how antibodies impact the development of primary B cell immune
128 responses we immunized mice with the Wuhan-Hu1 SARS-Cov2 receptor binding
129 domain (RBD) (Figure 2A). Antigen-specific antibodies were measured by ELISA
130 (Figures 2B-D). As expected, M-only mice were limited to the IgM isotype, and mM-
131 only mice produced no serum antibodies in response to the immunization (Figures 2B-
132 D). The kinetics of the serological response in M-only mice was similar to WT (Figure
133 2D), but the total amount of antibody was lower when considering all isotypes (Figure
134 2B). Notably, whereas the total antibody levels in WT mice decreased over the 150-
135 day period of observation, serum Ig levels were relatively stable and even increased
136 modestly in M-only mice (Figure 2B).

137 Germinal center responses were analyzed by flow cytometry on days 7, 14, 21
138 and 28. The absolute numbers of B cells and the relative proportions of germinal center
139 B cells among B220$^+$ B cells was similar among WT, M-only and mM-only mice at all
140 time point points analyzed (Figures 2E-F, Supp.Fig.2A). Thus, the contribution of
141 antibodies to GC magnitude and kinetics in the primary response to SARS-CoV2-RBD
142 appears to be limited.

143 Plasma cell precursors were evident in GCs of all 3 strains, but showed
144 increased caspase expression in mM-only mice and these mice had few detectable
145 mature plasma cells in lymph nodes (LNs) or bone marrow (Figures 2G-J). The data
146 are consistent with the idea that plasma cells that are unable to secrete antibody die
147 by apoptosis (Iwakoshi, Lee and Glimcher, 2003; Todd *et al.*, 2009; Bonaud *et al.*,
148 2023).

149 We analyzed the antigen-binding capacity of GC B cells in the primary response
150 by flow cytometry using the Wuhan-Hu1 RBD labeled with 2 different fluorophores
151 (Figure 2K-L). At the peak of the GC response, 14 days after immunization, there were
152 similar proportions of RBD-binding cells in WT and M-only mice (35 % and 26 %
153 respectively), but significantly more in the GCs of mM-only mice (45 % p=0.0021, Fig
154 2L). Moreover, whereas antigen binding B cells decreased over time in WT and M-
155 only mice they persisted in mM-only GCs (Figure 2L). The data is consistent with the
156 idea that secreted antibodies mask immunodominant epitopes and increase antigen
157 valency, thus curbing the relative competitive advantage of high affinity
158 immunodominant antigen binding cells in the later stages of the primary GC reaction
159 (Heyman, 2000; Andrews *et al.*, 2015; Schaefer-Babajew *et al.*, 2023; Cyster and
160 Wilson, 2024; Yan *et al.*, 2025).

161 To gain further insights into the effect of antibodies on primary GC responses
162 we examined clonality, diversity and IgV gene usage by single cell VDJ sequencing
163 14 days after immunization. As expected expanded clones of B cells were found in
164 GCs of all 3 genotypes (Figure 3A). However, the individual clones appeared to be
165 larger and less diverse in the GCs of mM-only mice than in mice that expressed
166 secreted antibodies. Consistent with this observation mM-only GC B cells showed
167 reduced Shannon and Inverse Simpson diversity indices, but similar levels of somatic
168 mutation compared to their counterparts (Figures 3B-D). Moreover, in contrast to the
169 follicular compartment, Ighv gene usage was strongly skewed to *Ighv1-74, ighv1-80,*
170 *Igkv14-111, Igkv2-109* and *Igkv4-55* in mM-only mice (Figure 3E). In conclusion,
171 secreted antibodies appear to be essential for the development of optimal diversity in
172 primary GC responses to SARS-CoV2 RBD – a mechanism that appears to be
173 significant even at the early stages of the response.
174
175 **Secondary Immune Responses**
176 To determine whether antibodies developing during the primary response influence
177 subsequent booster responses, we vaccinated WT, M-only and mM-only mice in
178 accordance with protocols used during human immunization against SARS-CoV2
179 using full-length stabilized SARS-Cov2 spike protein (Figure 4A).
180 Serum antibody responses were measured by ELISA at approximately weekly
181 intervals from days 6 to 97 after immunization. As in the primary responses, antibodies
182 were not detectable in mM-only mice (Figure 4B and Supp. Fig. 4A), and M-only mice
183 produced approximately 30-fold less serum antibody compared to WT mice at the
184 peak of the response. Flow cytometry on cells obtained from draining lymph nodes

185 showed that M-only and mM-only mice had overall similar proportions of GC B cells
186 (Figure 4C). Thus, the complete absence of secreted antibodies does not impact the
187 ability to form or sustain secondary GCs.

188 Antigen binding GC B cells were enumerated using fluorescently labeled
189 Wuhan-hu1 RBD since this is the primary target of the anti-Spike immune response in
190 mice and humans. Notably, the 3 strains differed significantly in the fraction of Wuhan-
191 Hu1 RBD binding B cells (Figure 4D-E). Whereas only 1.9 % and 3 % of the B cells in
192 WT or M-only GCs bound to RBD, 22 % of mM-only GC B cells showed demonstrable
193 binding (p= 0.002, Figure 4D).

194 To determine the antigen binding specificity of GC B cells that develop after
195 boosting, we cloned and expressed 146 representative antibodies and tested them for
196 binding to Wuhan-Hu1 spike and the isolated RBD by ELISA (Supplementary Table
197 2). Altogether, only 17 % (wild-type) and 25 % (M-only) of mAbs isolated from
198 secondary GCs exposed to endogenous antibodies showed measurable binding to the
199 immunising antigen, whereas 54 % of the mAbs isolated from mM-only GCs were of
200 sufficiently high affinity to bind by ELISA (Figure 4E and Supp. Fig. 3B). Whereas 32 %
201 of antibodies obtained from mM-only mice bound to the immunodominant RBD, only
202 4.2 % and 2.1 % of mAbs from WT and M-only GCs did so, respectively (p=0.0002
203 and 0.0005 respectively, Figure 4E). The fraction of antibodies binding to non-RBD
204 epitopes on the spike was 12.5 %, 23 % and 22 % in WT, M-only and mM-only mice,
205 respectively. To examine the nature of the antibodies produced after booster
206 immunization, we examined the Ig sequences from single cells. Despite similar
207 numbers of somatic mutations (Supp. Fig. 3C), GC B cells obtained from secondary
208 GCs of mM-only mice were more clonal and significantly less diverse than those

209 obtained from M-only mice with notable enrichment in *Ighv1-53* and *Ighv2-91* (Figures
210 4F-H). The data suggest that antibody feedback inhibits accumulation of GC B cells
211 that are restricted to the initial immunodominant epitope even when those antibodies
212 are restricted to the IgM isotype and when total Ig concentrations are 30-fold lower
213 than physiologic.

214 To determine whether passively transferred antibodies are sufficient to revert
215 the mM-only phenotype we repeated the prime boost experiment with Wuhan-Hu1
216 spike and transferred contemporaneous serum from WT mice into mM-only recipients
217 (Figure 5A). As determined by ELISA serologic reconstitution was only partial with an
218 approximately 10-fold lower level of specific antibodies in the mM-only recipients
219 compared to their WT counterparts (Supp Fig. 4A). Notably, passive antibody transfer
220 completely reverted the mM-only phenotype resulting in near complete loss of Wuhan-
221 Hu1 RBD binding B cells in the mM-only GCs. We conclude that secreted antibodies
222 make a significant contribution to the specificity and diversity of polyclonal germinal
223 center responses.

224 Sequential immunization strategies designed to produce broadly neutralizing
225 antibodies (bNAbs) to HIV-1 and Influenza virus are currently being investigated in
226 animal models and in the clinic. The multi-step vaccine concept being tested involves
227 priming to recruit rare bNAb precursors followed by iterative administration of
228 progressively more mutated antigens to shepherd B cell responses through a series
229 of somatic mutations required to produce bNAbs (Escolano *et al.*, 2016; Burton, 2019;
230 Haynes *et al.*, 2023). This idea has yet to produce necessary protective serologic
231 responses in part because “off target” antibodies dominate the response after booster
232 vaccination (Escolano *et al.*, 2019, 2021). To determine how circulating antibodies

233 might contribute to this effect, we immunized mice with a series of 4 HIV-1 CD4-binding
234 site-targeting immunogens, from which the first one is currently in early clinical testing
235 (NCT05471076; 426c.DMRS.Core (TM4) antigen, Figure 6A) (McGuire *et al.*, 2016).
236 Longitudinal ELISA analysis for antibodies binding to 426c.DMRS.Core showed that
237 titers were present throughout the immunization protocol in WT and M-only but not
238 mM-only mice (Figure 6B).

239 GC B cell numbers and somatic mutations were equivalent among the 3 mouse
240 strains with median GC B cell frequencies between 1.7 % to 2.2 % of all B cells in the
241 draining lymph node (Figure 6C and Supp. Fig. 6A). Several Igv genes were used
242 preferentially by all 3 groups but at variable frequencies, with only *Igkv1-135* uniquely
243 overrepresented in the mM-only group (Figure 6E and Supp. Fig. 6B). Considering all
244 cells irrespective of HIV-1 antigen-binding, we saw a high degree of clonality in all 3
245 groups (Figures 6F-G). Notably, there were very few TM4-binding cells in WT and M-
246 only mice but they constituted on average 9 % of all GC B cells in mM-only mice
247 (Figure 6H and Supp. Fig. 5C). Thus, only mM-only mice that are devoid of circulating
248 antibodies show significant levels of antigen-binding GC B cells after a sequential
249 series of HIV-1 vaccine boosters.

250

251

252 Discussion

253 GCs are microanatomic compartments specialized for affinity maturation and
254 diversification of humoral immune responses. Affinity maturation is an iterative process
255 involving repetitive cycles of division and mutation in the GC dark zone followed by
256 migration to the light zone where B cells test their newly acquired antigen receptors

257 for binding and capture of antigen deposited in follicular dendritic cells. Selection is
258 mediated by a combination of B cell receptor signaling and T follicular help (Victora
259 and Nussenzweig, 2022; Chen *et al.*, 2023). How GCs diversify antibody responses in
260 the face of strong positive selection is less well understood. Our data indicate that
261 even small amounts of specific antibodies produced during the immune response are
262 sufficient to diversify the GC by masking responses to immunodominant epitopes and
263 by producing immune complexes that lower the affinity thresholds for B cell entry into
264 the GC.
265
266 Antibody feedback has been studied primarily by passive antibody transfer in animals
267 and humans (Heyman, 2000; Cyster and Wilson, 2024). These experiments revealed
268 that both IgM and IgG can produce immune complexes and mediate masking through
269 interactions with Fc and complement receptors (Heyman, 2000). Moreover, recent
270 work in antibody knock in mice producing antibodies of differing affinity to a selected
271 epitope showed that the antibody feedback effects were dependent on affinity and that
272 changes in the T cell compartment might also contribute (Barbulescu *et al.*, 2025; Yan
273 *et al.*, 2025). Our experiments extend these findings to primary and secondary immune
274 responses in animals that have an otherwise intact polyclonal B and T cell
275 compartment but are unable to produce secreted antibodies. Our data show that
276 antibody feedback is a major mechanism for diversification of both primary and
277 secondary immune responses.
278
279 Diversification by antibody feedback has the potential to enable recall responses to
280 rapidly evolving pathogens. For example, although initial responses to SARS-CoV-2

281 were focused on highly strain specific epitopes, antibody feedback diversified the
282 response to include more conserved epitopes that offered some protection against
283 newly arising variants. However, our data indicate that these feedback effects pose a
284 very significant barrier to sequential immunization approaches such as those being
285 tested for HIV-1 that aim to focus immunity to a singular broadly neutralizing epitope.
286

287 ## Methods

288 ### Mice

289 C57BL/6J mice were purchased from Jackson Laboratories. M-only and mM-only mice
290 were created and maintained at the Rockefeller University with assistance from the
291 Rockefeller University CRISPR and Genome Editing Center and Transgenic and
292 Reproductive Technology Center. Cas9 (IDT) and sgRNA (IDT) ribonucleoprotein
293 complexes targeting the IgH locus were electroporated into C57BL6/J single cell
294 mouse embryos, which were then recovered and incubated overnight at 37 °C before
295 implantation into female foster mother mice. For M-only mice sgRNA with spacer
296 sequences GTAGATCTCTTCCTAAGAGG and TTACTAGGCTCCTCCATATG were
297 used to delete *Ighd–Igha*. M-only mice were retargeted and with sgRNAs with spacer
298 sequence CGCCTGTGTCAGACATGATC and GGGTAGGACAAGCAACGCAC to
299 delete the part of *Ighm* exon 4 only found in the secreted IgM splice form, as well as
300 the subsequent stop codon and alternative, intronic polyadenylation site (Danner and
301 Leder, 1985; Boes *et al.*, 1998; Ehrenstein *et al.*, 1998; Waisman *et al.*, 2007). Cutsite
302 adjacent deletions were verified by PCR from tail DNA and Sanger sequencing of PCR
303 products. Sequences were analyzed using Geneious Prime (GraphPad). Mice were
304 bred to homozygosity. Presence or absence of antibody isotypes was verified by flow

305 cytometry and ELISA of serum in homozygous animals from homozygous parents due
306 to maternal transfer of antibodies in utero and through suckling.
307 Male and female mice aged 6-12 weeks were used. Animals were housed at the
308 Rockefeller University Comparative Bioscience Center and all animal procedures were
309 performed following protocols approved by the Rockefeller University Institutional
310 Animal Care and Use Committee. Animals were housed at an ambient temperature of
311 22 °C and a humidity of 30–70 % under a 12 h–12 h light–dark cycle with free access
312 to food and water. For experimental endpoints, mice were euthanized using CO_2,
313 followed by cervical dislocation.
314
315 **Immunization**
316 Immunizations were performed by subcutaneous footpad injection of 5 μg of
317 immunogen in 33 % alhydrogel (Invivogen).
318
319 **Antibody infusion**
320 Serum was obtained from equally immunized, time-matched C56BL/6J mice and
321 administered to recipients i.v. within 6 h of harvest.
322
323 **Flow cytometry**
324 For steady-state experiments, mice aged from 10 to 11 weeks were sacrificed and
325 their spleen, mesenteric LN, Peyer's patches and bone marrow were isolated and
326 dissociated to obtain single-cell suspensions. Bone marrow from pelvic bone, femur
327 and tibia was isolated by centrifugation at 10,000 g for 15s. Spleen and Peyer's
328 patches were forced through a 70 μm cell strainer. LNs were collected into 1.5 mL

329 Eppendorf tubes and dissociated using a pestle. Spleen and bone marrow pellets were
330 then incubated in ACK lysis buffer for 15 min on ice, washed and processed together
331 with the LN as described below.
332 For all experiments, single cell suspensions were incubated in Fc block (BD
333 Biosciences) for 15 min. Cells were then centrifuged at 350 g for 5 min and
334 resuspended and incubated in a solution of PBS diluted fluorescent-Biotin-antigen
335 tetramers for 30 min on ice. Additional labeled antibodies were then added to the cells
336 and samples were incubate for 30 additional minutes on ice. For intracellular staining
337 of Caspase 3, cells were permeabilized using BD Foxp3 permeabilization kit, washed
338 in the supplied permeabilization buffer and stained for 30 min at 4 °C. as per
339 manufacturer's instructions.
340 Antigen tetramer staining was performed with a combination of two different
341 fluorescently-labelled streptavidins per antigen. Biotinylated antigens at 5 μg/mL were
342 individually pre-incubated with each streptavidin-fluorophore (all Biolegend) at a 1
343 μg/mL dilution before staining to allow tetramer formation, then combined and cells
344 resuspend in the mixture and incubated for 30 min on ice, before staining for other
345 surface markers. Samples were acquired on a BD LSRFortessa or BD Symphony A3
346 or A5. All cell sorting was performed on the BD FACSymphony S6. Data was analyzed
347 using FlowJo 10.10.0.
348
349 **Recombinant protein production**
350 All expression vectors for recombinant protein production were confirmed by Sanger
351 (Azenta) or Oxford Nanopore sequencing (Plasmidsaurus). The construct encoding
352 the RBD of SARS-CoV-2 (GenBank MN985325.1; S protein residues 319–539) was

353 previously described (Barnes *et al.*, 2020). All recombinant proteins were produced in
354 Expi293F cells (Gibco, A14527), except 426c.WT.SOSIP which was produced in
355 Expi293F GnTI- cells (Gibco, A39240). Transient transfections of expression plasmids
356 were performed using Expifectamine 293 transfection kit (Gibco, A14525) as
357 previously described (McGuire *et al.*, 2014). In brief, 4-6 days post transfection, culture
358 supernatant was harvested, centrifuged to pellet cells and sterilized by filtration for
359 affinity chromatography. Trimeric Env proteins were purified by passing the
360 supernatant through an agarose-bound *Galanthus nivalis* lectin (GNL) resin (Vector
361 Laboratories) and subsequent size-exclusion chromatography (SEC). A Ni Sepharose
362 6 Fast Flow resin (Cytiva, 117531803) was used for purification of His-tagged proteins.
363 Native gel electrophoresis identified peak fractions from size-exclusion
364 chromatography. Fractions corresponding to monomeric Envelope trimers, Spike S6P
365 protein trimers or RBD monomers were pooled and stored at -20 °C. Antibodies were
366 purified over a protein G Sepharose 4Fast Flow resin (Cytive 70611805) and buffer
367 exchanged into PBS and stored at -80 °C.
368 For random biotinylation, proteins were biotinylated using the EZ-Link-Sulfo-NHS-LC-
369 Biotinylation kit according to the manufacturer's instructions (Thermo Fisher Scientific,
370 31497). Excess biotin was removed by diafiltration with 100 kDa cutoff. Biotinylated
371 protein was stored at -20 °C or -80 °C.
372 Avi-tagged TM4 core gp120 or RBD were biotinylated using a BirA reaction according
373 to the manufacturer's instructions using a 5-fold molar excess of biotin (Avidity,
374 EC6.3.4.15), buffer exchanged to PBS and stored at -80°C.
375
376

377 **ELISA**

378 All ELISAs used Costar 96-well, half area, high binding, polystyrene assay plates
379 (Corning, Cat.# 3960), which were coated with the indicated antigen (TM4, SARS-
380 CoV-2 Wuhan-hu1 RBD or spike protein, all produced in house) or anti-isotype
381 antibody (anti-IgM, Southern Biotech, 1020-01; anti-IgG3, Southern Biotech, 1100-01;
382 anti-IgG1, Southern Biotech, 1070-01; anti-IgG2b, Southern Biotech, 1090-01; anti-
383 IgG2c, Jackson Immunoresearch, 115-005-208; anti-IgA, Southern Biotech, 1040-01)
384 at 2 – 5 μg/mL in PBS over night at 4°C. Plates were blocked with 5 % skimmed milk
385 powder in PBS or 1 % BSA 0.1 mM EDTA 0.05 % Tween20 in PBS for 2 h at room
386 temperature. 6 washes in PBS 0.05 % Tween 20 were performed after every
387 subsequent step. Sera were diluted in PBS at 1:50 to 1:100 top dilution and 1:3 (naïve
388 and after prime) or 1:4 (after boosts) or 1:5 (steady state serum antibody levels) serially
389 diluted for an 8-point curve. Isotype antibody standards (Southern Biotech 5300-01B)
390 were diluted to 10 μg/mL and diluted 1:5 in PBS for an 8-point curve. Secondary
391 antibodies conjugated to horseradish peroxidase were used to detect bound
392 antibodies mouse IgG (1:5000, Jackson ImmunoResearch Cat.# 115-035-071 or
393 Southern Biotech Cat.# 1030-05) or mouse IgM, IgG3, IgG1, IgG2b, or IgA (Southern
394 Biotech Cat.# 5300-05B) or IgG2c (Jackson ImmunoResearch 115-035-208) or total
395 Ig (anti-kappa combined with anti-lambda light chain, Southern Biotech Cat.# 5300-
396 05B). HRP substrate 3,3',5,5'-tetramethylbenzidine substrate (ThermoFisher, Cat.#
397 34021) was used for development and the reaction was stopped adding an equal
398 volume of 1 M H_2SO_4 (Sigma). Absorbance was read at 450 nm and 570 nm on a
399 FLUOstar Omega (BMG Labtech). For analysis of steady-state antibody concentration
400 in serum, isotype standards were included on every plate and used to fit a sigmoidal

401 4-parameter logistic regression standard curve in GraphPad Prism 10 which was used
402 to interpolate serum concentrations from dilutions in the exponential phase of the
403 curve. For total anti-antigen responses, sigmoidal 4-parameter logistic regression was
404 fitted to curves of every sample and used to calculate the half maximal binding titer
405 (BT_{50}). μg/mL values below detection were set to minimum detection level based on
406 control sera to avoid plotting 0 on logarithmic plots. For samples were signal was too
407 low for a curve fit BT_{50} was set to 10, which is 5x above the highest measured dilution.
408

409 **10x genomics and single-cell libraries**

410 Indicated mice were immunized with either Spike, RBD or HIV proteins. Cell
411 suspensions were prepared as mentioned before from popliteal lymph nodes and
412 samples were indexed using TotalSeqC cell surface antibodies (Biolegend). Live,
413 lineage$^-$ B cells (CD38$^+$, GC B cells RBD$^+$ and GCB RBD$^-$), and PC were then isolated
414 flow cytometry and loaded onto the Chromium Controller from 10x Genomics. scRNA-
415 seq libraries were prepared using the Chromium Single Cell 5′ v.2 Reagent Kit (10x
416 Genomics) according to the manufacturer's protocol. Libraries were loaded onto a
417 Illumina NovaSeq for single-cell gene expression (GEX), VDJ analysis and hashtags
418 (HTO) library at the Rockefeller University Genomics Resource Center. Hashtag
419 indexing from TotalSeqC antibodies was used to demultiplex the sequencing data and
420 generate gene and barcode matrices, respectively.

421 All single-cell BCR libraries were mapped to the Cell Ranger VDJ GRCm38 reference
422 using Cell Ranger multi v.8.1.0 (10x genomics). Contigs containing less than 50 reads
423 and more than one heavy or light chain were removed. Antibodies heavy and light
424 chains were paired and analyzed using igpipeline v.3.0

425 (https://github.com/stratust/igpipeline/tree/igpipeline3), previously described (Wang *et*
426 *al.*, 2023), with the mouse IMGT database as reference (Lefranc, 2011).
427 For the primary response dataset analyses (Fig. 3), scRNA-seq and Hashtag-oligos
428 unique molecular identifier quantification were performed with Cell Ranger multi
429 v.8.0.1 using the Cell Ranger GEX reference mm10, and analyzed in R with Seurat
430 v.5.1.0 (Hao *et al.*, 2021). Cells were demultiplexed with MULTISeqDemux, and those
431 classified as doublets or with mitochondrial content greater than 10 % and feature
432 count less than 1,000 or greater than 6,500 were excluded. Cell cycle genes were
433 regressed out. Sample batches were then merged, scaled and normalized with
434 SCTransform. B cell (*Cd19, Ms4a1, Cd79a, Tnfrsf13c, Aicda, Lyz2, Cd63*), Follicular
435 (*Cd38, Cd55, Bcl2, Maml2, Notch2, Gpr183, Sell, Ccr6*), and memory B cell (Binet *et*
436 *al.*, 2024) signatures were assigned using AddModuleScore. Cells with low B cell
437 module score (≤ 25th percentile) or with high memory B cell score (≥ 75th percentile)
438 were excluded. B cells expressing *Bcl6, Aicda, S1pr2* or *Fas* at high levels (≥ 75th
439 percentile) were classified as GC B cells, whereas those with high follicular score (≥
440 75th percentile) were classified as follicular B cells.
441
442 **Statistical analysis**
443 Details of statistics including tests used, exact values and n numbers are indicated in
444 figure legends and/or main text. Quantification and statistical analyses were performed
445 in R (v4.4.0) with Rstudio server (2024.04.0 Build 735) and/or GraphPad Prism
446 (Version 10.2.3), unless otherwise detailed in this methods section. For all boxplots,
447 the central line denotes the median, the box represents the interquartile range (IQR),
448 lower and upper whiskers denotate the data variability with minimum and maximum

449 data points, respectively, extending 1.5 x IQR from Q1/Q3. Graphs generated using
450 Prism and R were assembled into figures using Adobe Illustrator. Flow cytometry
451 analysis was performed in FlowJo v.10.10.0 software (BD).
452

453 **Figures and figure legends**

Figure 1

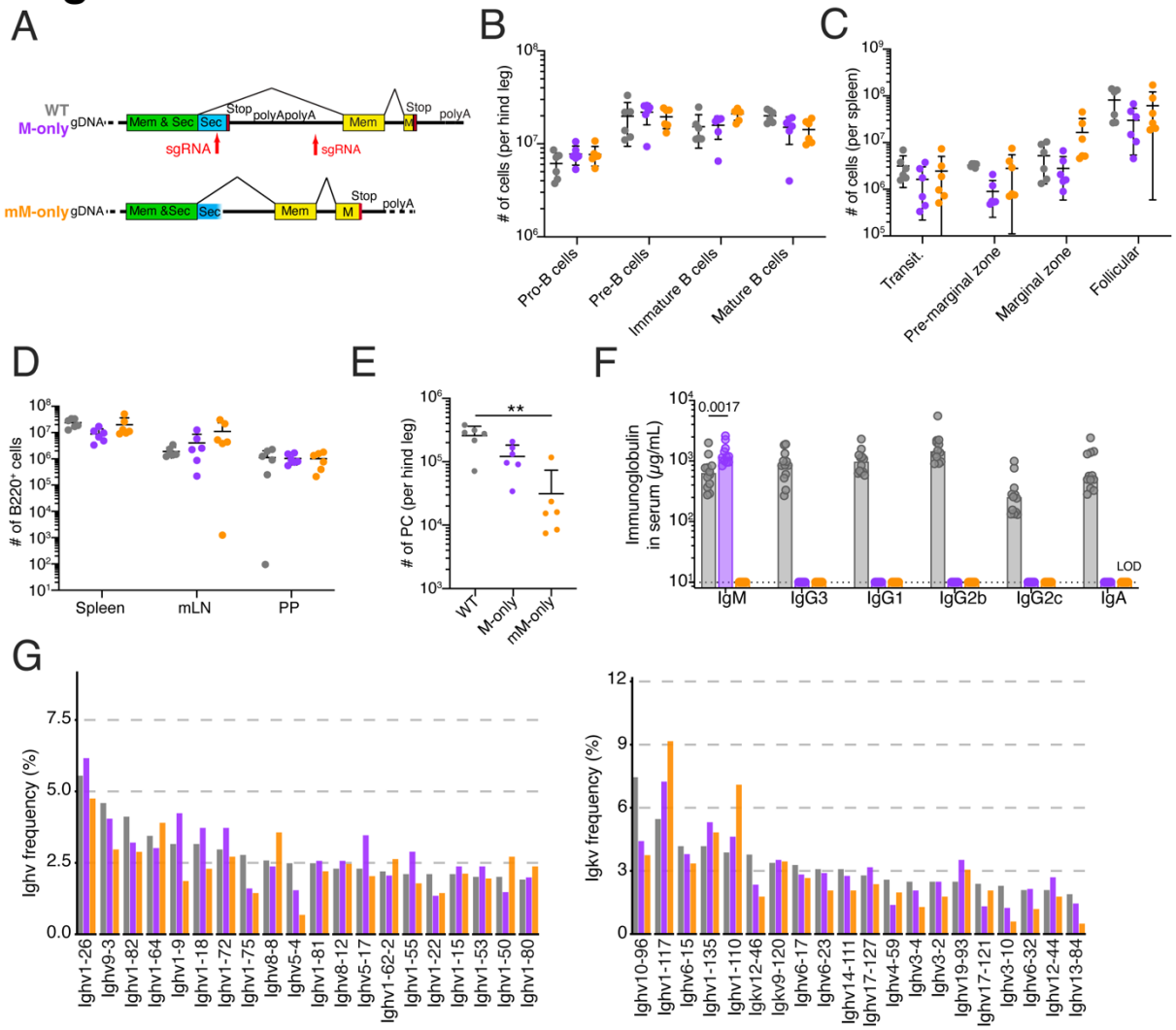

454

455

456 **Figure 1. B cell development in M-only and mM-only mice.** (**A**) Schematic shows
457 structure of *Ighm* exon 4 in M-only and mM-only mice. (**B**) Number of pro-, pre-,
458 immature and mature B cells in the bone marrow by flow cytometry. Gating as in
459 Supplementary Fig. 1A. (**C**) Number of the splenic B cell subsets by flow cytometry.
460 Gating on B220$^+$ cells as in Supplementary Fig. 1B. (**D**) Number of live B cells in
461 spleen, mesenteric lymph node (mLN) and Peyer's Patches (PP) by flow cytometry.
462 Gating on B220$^+$ cells as in Supplementary Fig. 1B-D. (**E**) Number of plasma cells in
463 the bone marrow of one leg by flow cytometry. (**F**) ELISA quantification of IgM, IgG3,
464 IgG1, IgG2b, IgG2c and IgA in the serum of WT, M-only and mM-only mice. (**G**) Ighv
465 (left panel) and Igkv (right panel) gene usage in follicular B cells. Data was pooled
466 from two independent experiments. Each dot or circle represents a mouse. Statistical
467 analysis was by non-parametric one-way ANOVA. All experiments were performed at
468 least twice. **$p < 0.01$. Bars indicate mean and standard deviation.
469
470
471

472

Figure 2

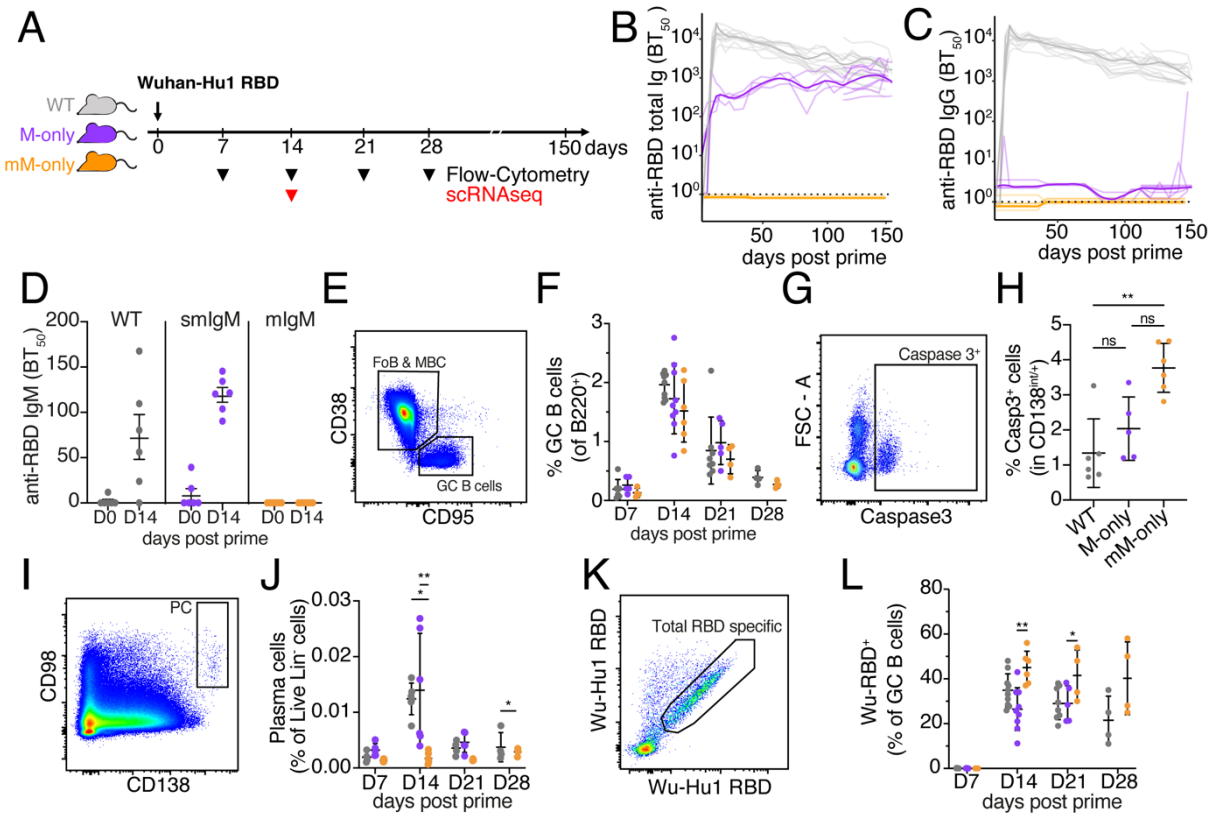

473

474

475 **Figure 2. Primary vaccine responses.** (**A**) Diagram of the experimental protocol. (**B**)
476 ELISA quantification of anti-RBD antibodies in the serum measured every 3 to 5 days
477 between D0 and D150. (**C**) As in (B) for anti-IgG anti-RBD antibodies in the serum.
478 Thin lines (in B and C) represent single mice, bold lines represent group mean. (**D**)
479 Serum anti-RBD IgM ELISA 0 or 14 after immunization. (**E**) Flow cytometric gating for
480 $CD38^{-}CD95^{+}$ GC cells. Pre-gated on $B220^{+}$ cells in draining lymph nodes (dLN). (**F**)
481 Quantification of GC B cells from (E) at the indicated time points after immunization.
482 Each dot represents one mouse. (**G**) Flow cytometry gating for $Caspase3^{+}$ cells among
483 $CD138^{int/+}$ live lin^{-} cells. (**H**) Quantification of (G) among $CD138^{int/+}$ live lin- cells in
484 draining LN at 14 days after immunisaiton. (**I**) Flow cytometric gating for $CD98^{+}$
485 $CD138^{+}$ PC pre-gated on live lin^{-} cells in the draining LN. (**J**) Quantification of (I) at the
486 indicated times after immunization. (**K**) Flow cytometric gating of RBD^{+} cells among
487 GC B cells in the draining LNs. Pre-gated for GC as in (E). (**L**) Quantification of (K) at
488 the indicatd time points after immunization. Each dot represents one mouse. Statistical
489 analysis using non-parametric one-way ANOVA. All experiments were performed at
490 least twice. Bars in (D, F, H, J and L) indicate mean ± standard deviation. $^{**}p < 0.01$,
491 $^{*}p < 0.05$.

Figure 3

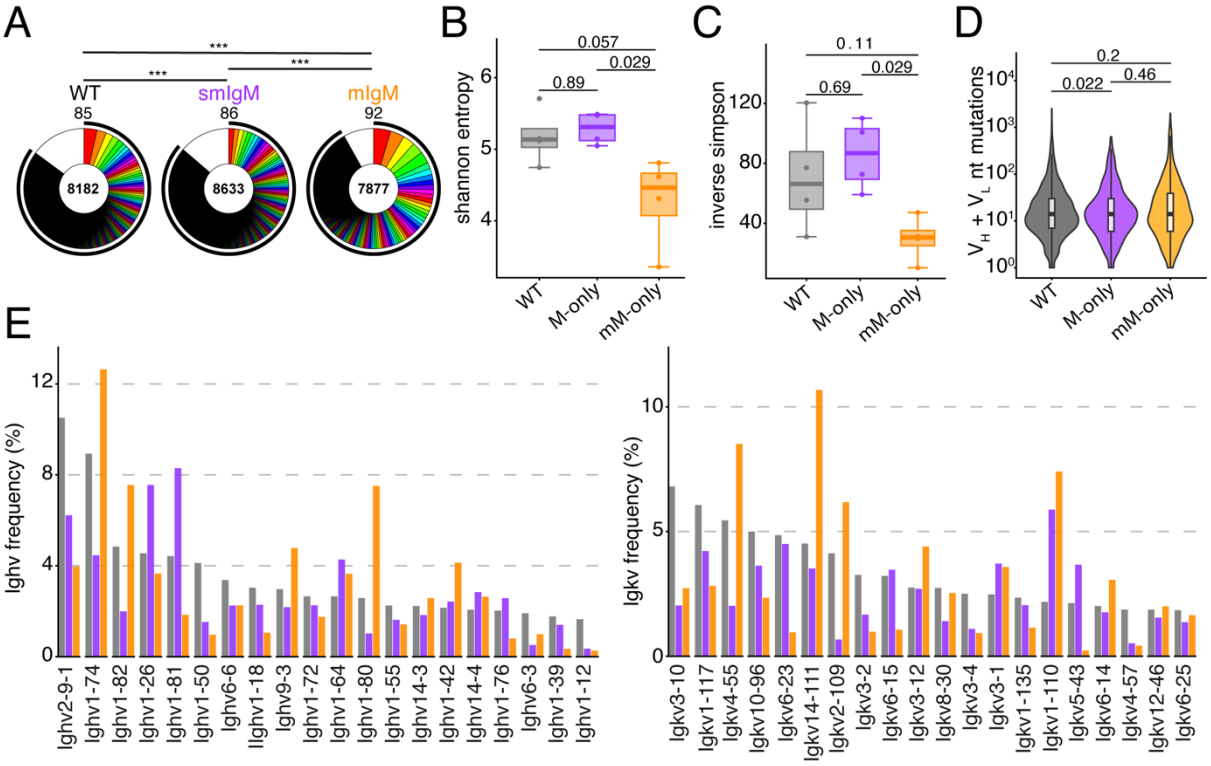
A
***
***
***
WT
85
8182
smIgM
86
8633
mIgM
92
7877
B
shannon entropy
0.057
0.029
0.89
WT
M-only
mM-only
C
inverse simpson
0.11
0.029
0.69
WT
M-only
mM-only
D
$V_H + V_L$ nt mutations
0.2
0.022
0.46
WT
M-only
mM-only
E
Ighv frequency (%)
Ighv2-9-1
Ighv1-74
Ighv1-82
Ighv1-26
Ighv1-81
Ighv1-50
Ighv6-6
Ighv1-18
Ighv9-3
Ighv1-72
Ighv1-64
Ighv1-80
Ighv1-55
Ighv14-3
Ighv1-42
Ighv14-4
Ighv1-76
Ighv6-3
Ighv1-39
Ighv1-12
Igkv frequency (%)
Igkv3-10
Igkv1-117
Igkv4-55
Igkv10-96
Igkv6-23
Igkv14-111
Igkv2-109
Igkv3-2
Igkv6-15
Igkv3-12
Igkv8-30
Igkv3-4
Igkv3-1
Igkv1-135
Igkv1-110
Igkv5-43
Igkv6-14
Igkv4-57
Igkv12-46
Igkv6-25

495 **Figure 3. Primary GC antibody sequences.** (**A**) Pie charts depicting the distribution
496 of antibody sequences obtained 14 days after prime immunization from GC B cells
497 from 4 mice/genotype. Inner circle numbers indicates the number of sequences
498 analyzed for each genotype. White indicates sequences isolated only once, colored
499 or black pie slices are proportional to the number of clonally related sequences. The
500 outlined black line indicates the percentages of cells in a clonal family. (**B**) Boxplots
501 showing shannon entropy scores for sequences depicted in (A). (**C**) Boxplots depicting
502 inverse Simpson index for sequences shown in (A). (**D**) Violin plots of V gene
503 mutations among sequences show in (A). (**E**) Bar graphs showing Ighv and Igkv gene
504 usage among sequences shown in (A). Sequences used to construct plots in panels
505 (M)-(Q) can be found in Supplementary Table 1. Statistics in (A) indicate chi-squared
506 test with Monte Carlo p-value simulation, p-values were subsequently corrected using
507 the Benjamini-Hochberg (BH) procedure. Statistics in (B)-(D) indicate two-sided Mann-
508 Whitney U test. ****$p<0.0001$, ***$p <0.001$,**$p <0.01$, *$p<0.05$. Each dot represent a
509 single mouse.
510

Figure 4

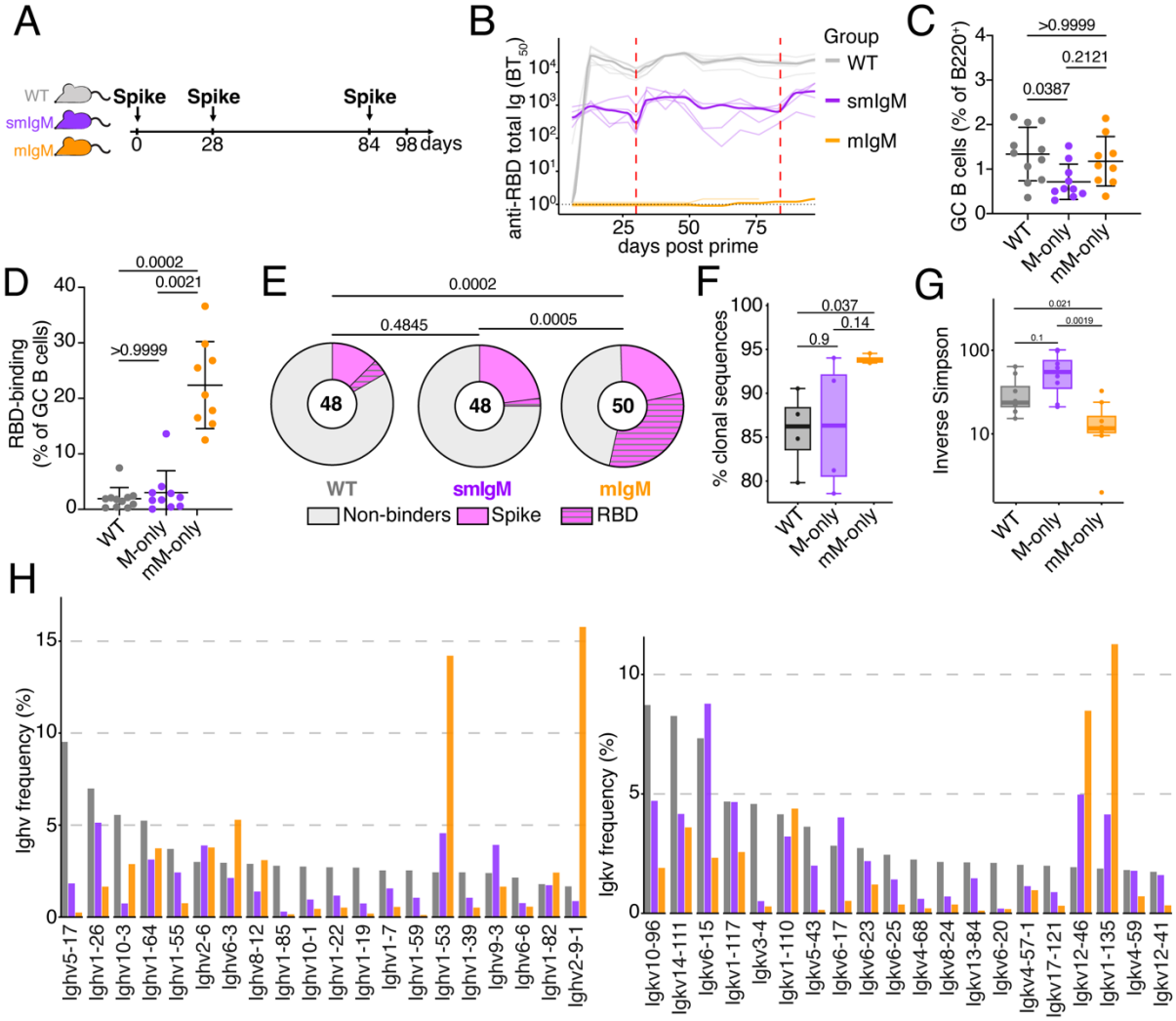
A
WT
smIgM
mIgM
Spike
Spike
Spike
0
28
84
98 days
B
anti-RBD total Ig (BT50)
days post prime
Group
WT
smIgM
mIgM
C
GC B cells (% of B220+)
>0.9999
0.2121
0.0387
WT
M-only
mM-only
D
RBD-binding (% of GC B cells)
0.0002
0.0021
>0.9999
WT
M-only
mM-only
E
0.0002
0.4845
0.0005
48
48
50
WT
smIgM
mIgM
Non-binders
Spike
RBD
F
% clonal sequences
0.037
0.14
0.9
WT
M-only
mM-only
G
Inverse Simpson
0.021
0.0019
0.1
WT
M-only
mM-only
H
Ighv frequency (%)
Ighv5-17
Ighv1-26
Ighv10-3
Ighv1-64
Ighv1-55
Ighv2-6
Ighv6-3
Ighv8-12
Ighv1-85
Ighv10-1
Ighv1-22
Ighv1-19
Ighv1-7
Ighv1-59
Ighv1-53
Ighv1-39
Ighv9-3
Ighv6-6
Ighv1-82
Ighv2-9-1
Igkv frequency (%)
Igkv10-96
Igkv14-111
Igkv6-15
Igkv1-117
Igkv3-4
Igkv1-110
Igkv5-43
Igkv6-17
Igkv6-23
Igkv6-25
Igkv4-68
Igkv8-24
Igkv13-84
Igkv6-20
Igkv4-57-1
Igkv17-121
Igkv12-46
Igkv1-135
Igkv4-59
Igkv12-41

514 **Figure 4. Prime boost vaccination.** (**A**) Diagram of the experimental protocol. (**B**)
515 ELISA quantification of total anti-RBD antibodies in the serum measured weekly from
516 D6 to D97 after prime immunization. Thin lines represent single mice, bold line
517 indicates group mean. Dashed red lines indicate booster immunizations. (**C**)
518 Percentage of GC B cells among $B220^+$ B cells in the draining LN at D98. Gating as
519 in (Fig. 2E). (**D**) Percentage of RBD-binding GC B cells in the draining LN at D98. Each
520 dot represents one mouse. Gating as in (Fig. 2K). (**E**) Pie charts depicting the
521 distribution of RBD-binding, Spike-binding or non-binding recombinant antibodies
522 cloned from the largest expanded clones of 4 mice/group of GC B cells on D98 from
523 draining LNs. $BT_{50} < 10$ μg/mLconsidered binders. Inner circle numbers indicate the
524 number of sequences analyzed. (**F**) Boxplots showing the percentage of clonal
525 sequences from GC B cells on Day 98 (**G**) Boxplots depicting the inverse Simpson
526 index for sequences from (F). (**H**) Bar graphs showing Ighv and Igkv gene usage
527 among sequences from (F). Statistics in F and G were determined using the Mann-
528 Whitney U test (two-sided). Bars in (C) and (D) indicate mean ± standard deviation..
529 All flow cytometry experiments were performed at least twice. Each dot represent a
530 single mouse.

Figure 5

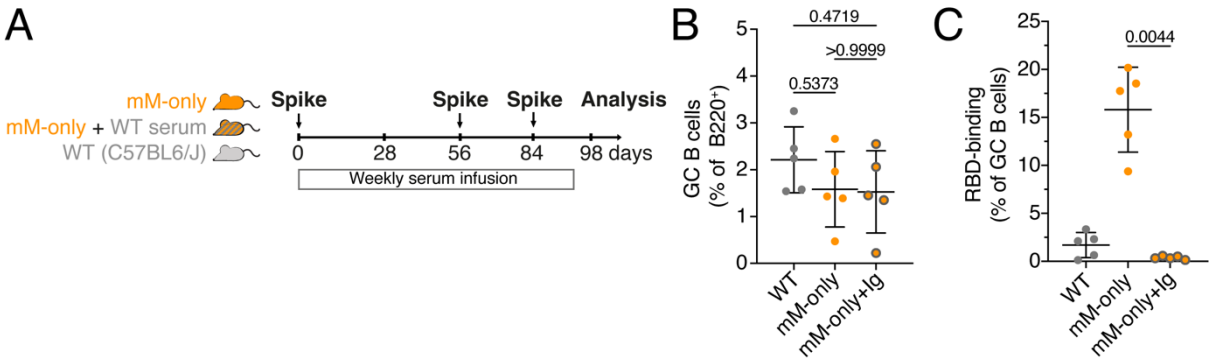

531

532

533

534 **Figure 5. Immune serum rescues the mM-only phenotype.** (**A**) Diagram of the
535 experimental protocol. (**B**) Percentage of GC B cells among B220^{+} B cells in the
536 draining LN on day 98. Each dot represents one mouse. Gating as in (Fig. 2E). (**C**)
537 Percentage of RBD-binding GC B cells. Each dot represents one mouse. Gating as in
538 (Fig. 2K). Bars indicate mean ± standard deviation. Statistical analysis was by non-
539 parametric one-way ANOVA. Each dot represent a single mouse.

Figure 6

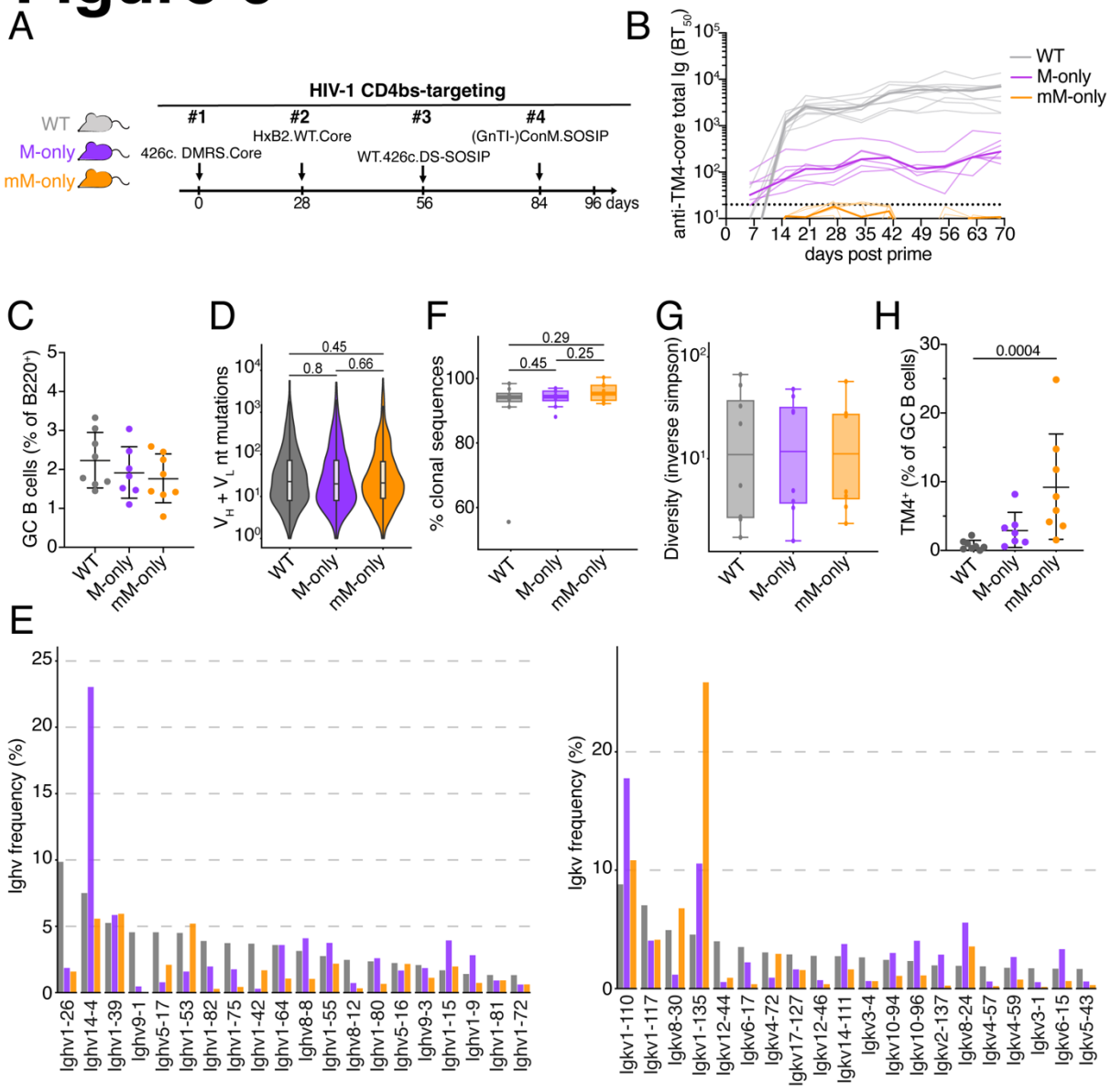
A
HIV-1 CD4bs-targeting
WT
M-only
mM-only
#1
426c. DMRS.Core
#2
HxB2.WT.Core
#3
WT.426c.DS-SOSIP
#4
(GnTI-)ConM.SOSIP
0
28
56
84
96 days
B
anti-TM4-core total Ig (BT50)
days post prime
WT
M-only
mM-only
C
GC B cells (% of B220+)
D
VH + VL nt mutations
0.45
0.8
0.66
F
% clonal sequences
0.29
0.45
0.25
G
Diversity (inverse simpson)
H
TM4+ (% of GC B cells)
0.0004
E
Ighv frequency (%)
Ighv1-26
Ighv14-4
Ighv1-39
Ighv9-1
Ighv5-17
Ighv1-53
Ighv1-82
Ighv1-75
Ighv1-42
Ighv1-64
Ighv8-8
Ighv1-55
Ighv8-12
Ighv1-80
Ighv5-16
Ighv9-3
Ighv1-15
Ighv1-9
Ighv1-81
Ighv1-72
Igkv frequency (%)
Igkv1-110
Igkv1-117
Igkv8-30
Igkv1-135
Igkv12-44
Igkv6-17
Igkv4-72
Igkv17-127
Igkv12-46
Igkv14-111
Igkv3-4
Igkv10-94
Igkv10-96
Igkv2-137
Igkv8-24
Igkv4-57
Igkv4-59
Igkv3-1
Igkv6-15
Igkv5-43

542 **Figure 6. Sequential immunization with an HIV-1 antigen series.** (**A**) Diagram of
543 the experimental protocol. (**B**) ELISA quantification of total anti-TM4-core serum
544 antibodies measured weekly from day 6 to 69. Thin lines represent single mice, bold
545 lines represent group mean. (**C**) Percentage of GC B cells among B220^{+} B cells in the
546 draining LN on day 96. Gating as in (Fig. 2E). (**D**) Violin plots showing somatic
547 hypermutation in GC B cells on day 98. (**E**) Bar graphs showing Ighv left panel) and
548 Igkv (right panel) gene usage in GC B cells on day 98. (F) Boxplots depicting the
549 percentage of clonal sequences from GC B cells on Day 98 (**G**) Boxplots depicting
550 Inversed Simpson index of antibody sequences from d98 GC B cells . (**H**) Percentages
551 of TM4 -binding GC B cells. Bars in (C) and (H) indicate mean ± standard deviation.
552 Statistical analysis was by non-parametric one-way ANOVA. Each dot represent a
553 single mouse.
554

Supplementary Figure S1

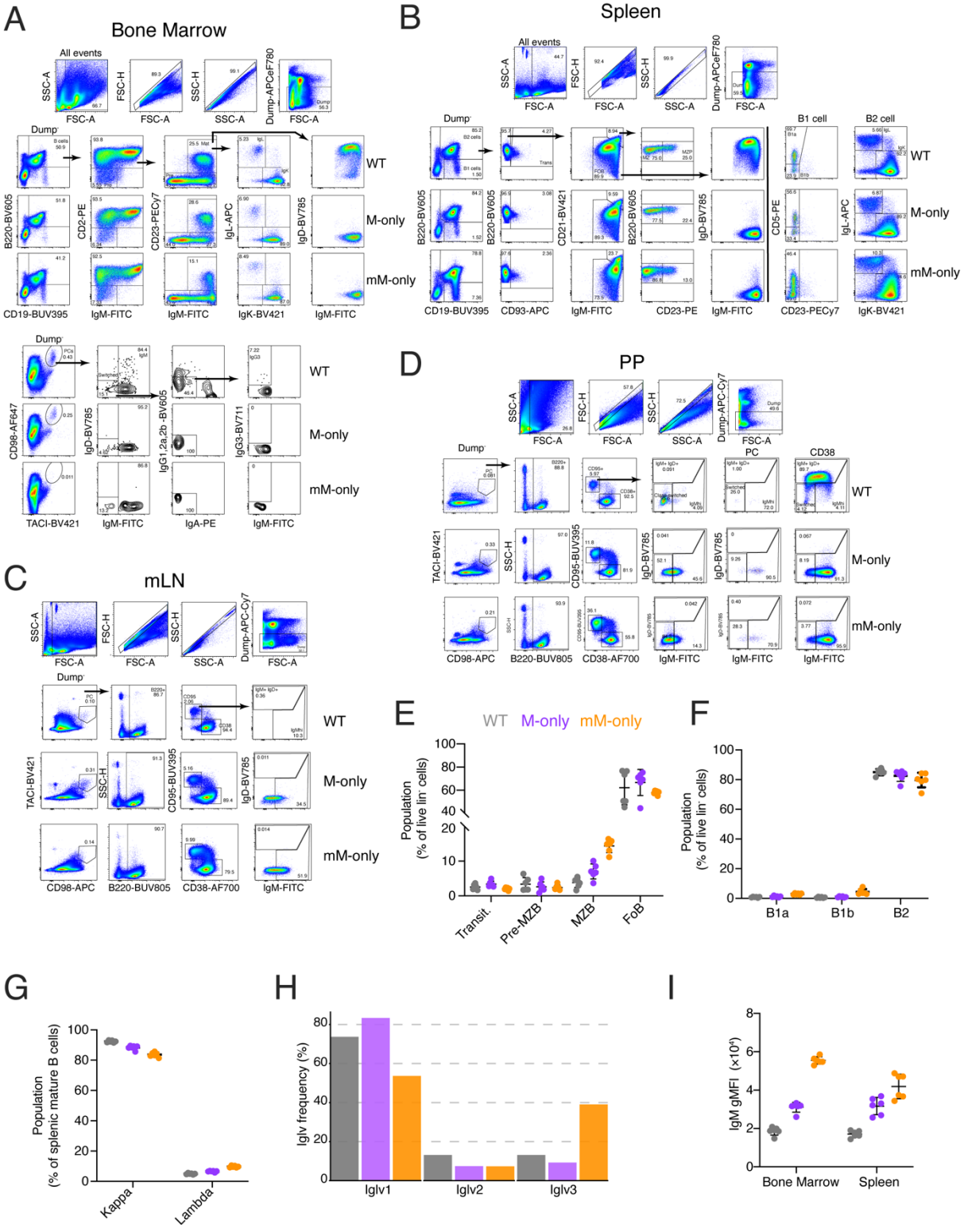

555

556

557

558 **Supplementary Figure 1.** Analysis of M-only and mM-only mosue strains. Related to
559 Figure 1. (**A**) Flow cytometric gating strategy in the bone marrow. (**B**) Flow cytometric
560 gating strategy in the spleen. (**C**) Flow cytometric gating strategy in the mesenteric LN
561 (mLN). (**D**) Flow cytometric gating strategy in the Peyer's patches (PP). (**E**)
562 Percentages of splenic, transitional (Transit), pre-marginal zone (Pre-MZB), marginal
563 zone (MZB) , and follicular (FoB) B cells among live lineage$^-$ cells. (**F**) Percentages of
564 splenic B1a, B1b amd B2 cells among live lineage$^-$ cells. (**G**) Percentages of splenic
565 kappa or lambda light chain bearing mature B cells. (**H**) Bar graphs showing Iglv gene
566 usage in follicular B cells. (*I*) Geometric mean fluorescence intensity (gMFI) of IgM-
567 FITC in the bone marrow mature B cells and splenic follicular B cells. Each dot
568 represent a single mouse. Bars indicate mean ± standard deviation.

569

Supplementary Figure S2

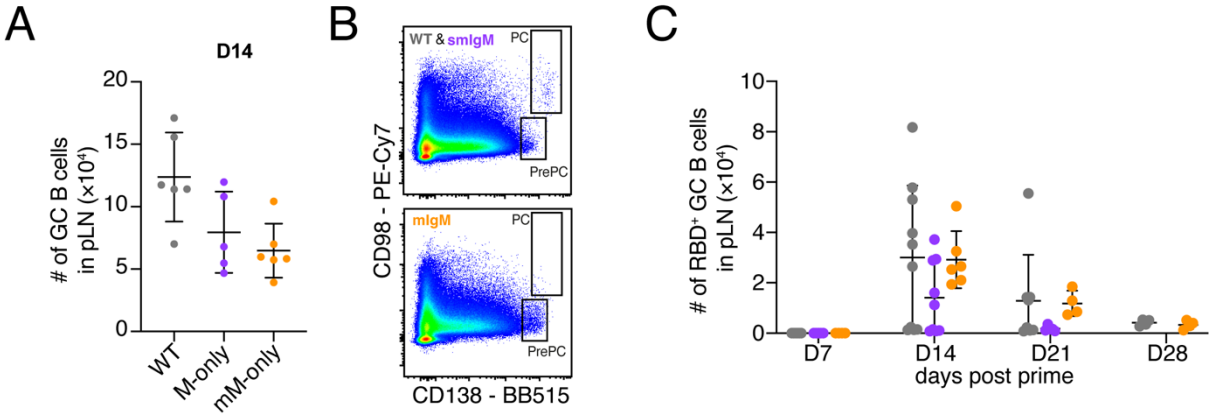

573 **Supplementary Figure 2. Prime immunization with RBD**. Related to Figure 2. (**A**)
574 Absolute numbers of GC B cells in draining LN 14 days after RBD immunization. (**B**)
575 Flow cytometric gating strategy for PC. (**C**) Numbers of RBD^+ GC B cells at D7, D14,
576 D21 and D28 after RBD immunization. Each dot represent a single mouse. Bars
577 indicate mean ± standard deviation.

578

Supplementary Figure S3

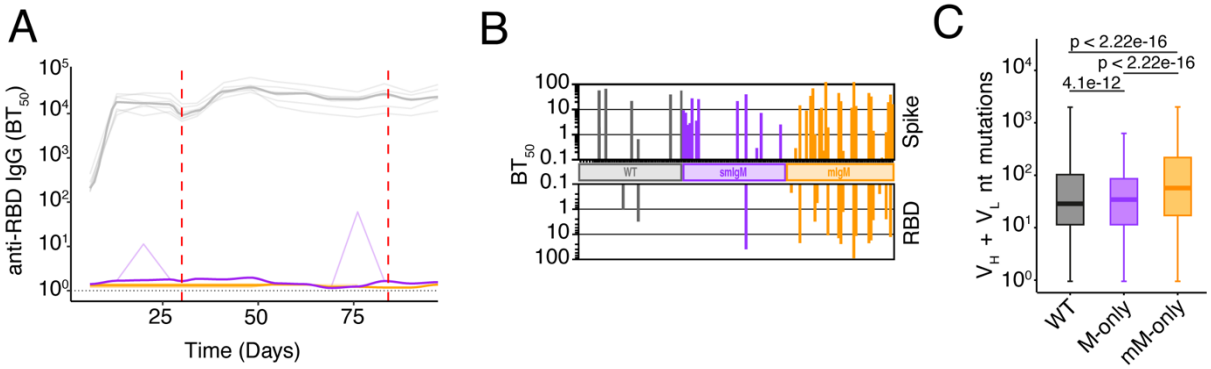

582 **Supplementary Figure 3. Analysis of anti-Spike prime boost responses.** Related
583 to Figure 4. (**A**) ELISA quantification of anti-RBD IgG antibodies in the serum of mice
584 from Figure 4 measured weekly from day 6 to day 97. (**B**) Bar graph of recombinant
585 antibodies binding to Spike (top) or RBD (bottom) protein. Each bar represents one
586 antibody. (**C**) Boxplots depicting somatic hypermutations in GC B cells on day 98 from
587 Figure 4 . P-value of two-sided Mann-Whitney U test indicated.
588
589

Supplementary Figure S4

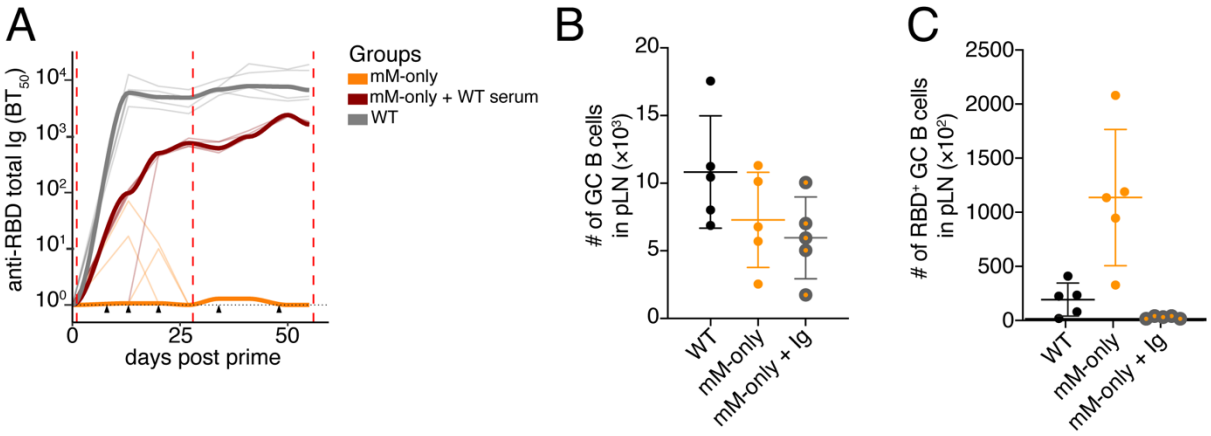

590

591

592

593 **Supplementary Figure 4. Analysis of serum transfer experiment.** Related to
594 Figure 5. (**A**) ELISA quantification of anti-RBD total Ig antibodies in the serum
595 measured weekly from day 0 to day 55. Red dashed lines indicate immunizations,
596 black triangles indicate serum transfer. Thin lines indicate individual mice, bold lines
597 indicate mean. (**B**) Number of GC B cells in dLN. (**C**) Number of RBD specific GC B
598 cells in dLN. Each dot represent a single mouse, bars indicate mean ± standard
599 deviation.
600
601
602

Supplementary Figure S5

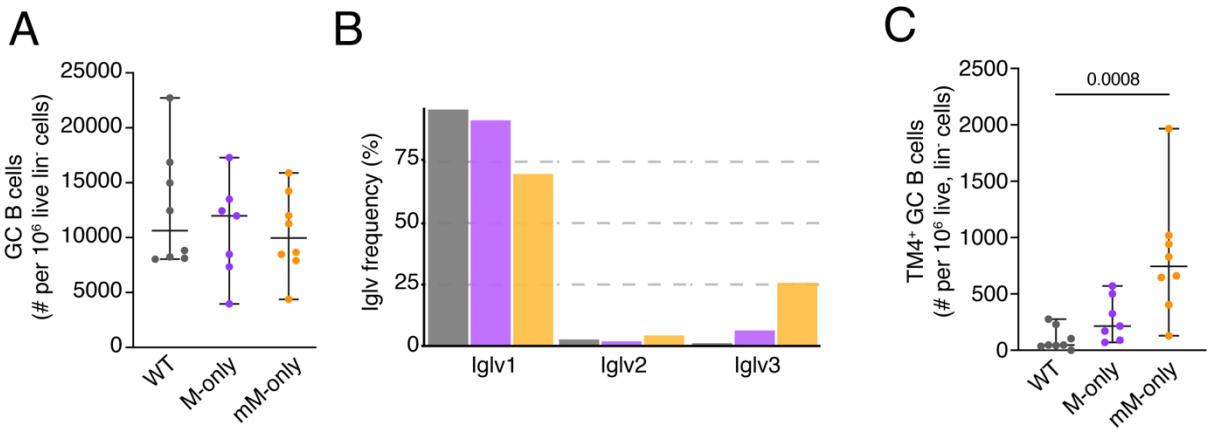

603

604

605

606 **Supplementary Figure 5. Analysis of anti-HIV-1 sequential immunization.**
607 Related to Figure 6. (**A**) Number of GC B cells, (**B**) Bar graphs showing Iglv gene
608 usage in GC B cells and (**C**) number of TM4-binding GC B cells in sequentially
609 immunized mice on day 96 in draining LNs. Each dot represent a single mouse, bars
610 indicate mean ± standard deviation.

References

Andrews, S.F. *et al.* (2015) “High Preexisting Serological Antibody Levels Correlate with Diversification of the Influenza Vaccine Response,” *Journal of Virology*. Edited by R.M. Sandri-Goldin, 89(6), pp. 3308–3317. Available at: https://doi.org/10.1128/JVI.02871-14.

Bannard, O. and Cyster, J.G. (2017) “Germinal centers: programmed for affinity maturation and antibody diversification,” *Current Opinion in Immunology*, 45, pp. 21–30. Available at: https://doi.org/10.1016/j.coi.2016.12.004.

Barbulescu, A. *et al.* (2025) “Antibody-mediated feedback modulates interclonal competition in the germinal center.” Immunology. Available at: https://doi.org/10.1101/2025.11.06.686519.

Barnes, C.O. *et al.* (2020) “Structures of Human Antibodies Bound to SARS-CoV-2 Spike Reveal Common Epitopes and Recurrent Features of Antibodies,” *Cell*, 182(4), pp. 828-842.e16. Available at: https://doi.org/10.1016/j.cell.2020.06.025.

Binet, L. *et al.* (2024) “Specific pre-plasma cell states and local proliferation at the dark zone - medulla interface characterize germinal center-derived plasma cell differentiation in lymph node.” Immunology. Available at: https://doi.org/10.1101/2024.07.26.605240.

Boes, M. *et al.* (1998) “Enhanced B-1 cell development, but impaired IgG antibody responses in mice deficient in secreted IgM,” *Journal of Immunology (Baltimore, Md.: 1950)*, 160(10), pp. 4776–4787.

Bonaud, A. *et al.* (2023) “Sec22b is a critical and nonredundant regulator of plasma cell maintenance,” *Proceedings of the National Academy of Sciences*, 120(2), p. e2213056120. Available at: https://doi.org/10.1073/pnas.2213056120.

Burton, D.R. (2019) “Advancing an HIV vaccine; advancing vaccinology,” *Nature Reviews Immunology*, 19(2), pp. 77–78. Available at: https://doi.org/10.1038/s41577-018-0103-6.

Chen, S.T. *et al.* (2023) “B cell receptor signaling in germinal centers prolongs survival and primes B cells for selection,” *Immunity*, p. S1074761323000778. Available at: https://doi.org/10.1016/j.immuni.2023.02.003.

Cyster, J.G. and Wilson, P.C. (2024) “Antibody modulation of B cell responses—Incorporating positive and negative feedback,” *Immunity*, 57(7), pp. 1466–1481. Available at: https://doi.org/10.1016/j.immuni.2024.06.009.

Dal Porto, J.M. *et al.* (2002) “Very Low Affinity B Cells Form Germinal Centers, Become Memory B Cells, and Participate in Secondary Immune Responses When Higher Affinity Competition Is Reduced,” *Journal of Experimental Medicine*, 195(9), pp. 1215–1221. Available at: https://doi.org/10.1084/jem.20011550.

Danner, D. and Leder, P. (1985) “Role of an RNA cleavage/poly(A) addition site in the production ofmembrane-bound and secreted IgM mRNA,” *Proceedings of the National Academy of Sciences*. Vol.82, December, pp. 8658–8662.

De Carvalho, R.V.H. *et al.* (2023) “Clonal replacement sustains long-lived germinal centers primed by respiratory viruses,” *Cell*, 186(1), pp. 131-146.e13. Available at: https://doi.org/10.1016/j.cell.2022.11.031.

Eckl-Dorna, J. *et al.* (2019) “Allergen-Specific Antibodies Regulate Secondary Allergen-Specific Immune Responses,” *Frontiers in Immunology*, 9, p. 3131. Available at: https://doi.org/10.3389/fimmu.2018.03131.

Ehrenstein, M.R. *et al.* (1998) “Targeted gene disruption reveals a role for natural secretory IgM in the maturation of the primary immune response,” *Proceedings of the National Academy of Sciences of the United States of America*, 95(17), pp. 10089–10093. Available at: https://doi.org/10.1073/pnas.95.17.10089.

ElTanbouly, M.A. *et al.* (2024) *Journal of Experimental Medicine*, 221(1), p. e20231838. Available at: https://doi.org/10.1084/jem.20231838.

Escolano, A. *et al.* (2016) “Sequential Immunization Elicits Broadly Neutralizing Anti-HIV-1 Antibodies in Ig Knockin Mice,” *Cell*, 166(6), pp. 1445-1458.e12. Available at: https://doi.org/10.1016/j.cell.2016.07.030.

Escolano, A. *et al.* (2019) “Immunization expands B cells specific to HIV-1 V3 glycan in mice and macaques,” *Nature*, 570(7762), pp. 468–473. Available at: https://doi.org/10.1038/s41586-019-1250-z.

Escolano, A. *et al.* (2021) “Sequential immunization of macaques elicits heterologous neutralizing antibodies targeting the V3-glycan patch of HIV-1 Env,” *Science Translational Medicine*, 13(621), p. eabk1533. Available at: https://doi.org/10.1126/scitranslmed.abk1533.

Hägglöf, T. *et al.* (2023) “Continuous germinal center invasion contributes to the diversity of the immune response,” *Cell*, 186(1), pp. 147-161.e15. Available at: https://doi.org/10.1016/j.cell.2022.11.032.

Hao, Y. *et al.* (2021) “Integrated analysis of multimodal single-cell data,” *Cell*, 184(13), pp. 3573-3587.e29. Available at: https://doi.org/10.1016/j.cell.2021.04.048.

Haynes, B.F. *et al.* (2023) “Strategies for HIV-1 vaccines that induce broadly neutralizing antibodies,” *Nature Reviews Immunology*, 23(3), pp. 142–158. Available at: https://doi.org/10.1038/s41577-022-00753-w.

Heyman, B. (2000) “Regulation of Antibody Responses via Antibodies, Complement, and Fc Receptors,” *Annual Review of Immunology*, 18(1), pp. 709–737. Available at: https://doi.org/10.1146/annurev.immunol.18.1.709.

Inoue, T. *et al.* (2021) “Exit from germinal center to become quiescent memory B cells depends on metabolic reprograming and provision of a survival signal,” *Journal*

686 *of Experimental Medicine*, 218(1), p. e20200866. Available at:
687 https://doi.org/10.1084/jem.20200866.

688 Inoue, T., Shinnakasu, R. and Kurosaki, T. (2022) “Generation of High Quality
689 Memory B Cells,” *Frontiers in Immunology*, 12, p. 825813. Available at:
690 https://doi.org/10.3389/fimmu.2021.825813.

691 Ise, W. and Kurosaki, T. (2020) “Regulation of Plasma Cell Differentiation,” in J.-Y.
692 Wang (ed.) *B Cells in Immunity and Tolerance*. Singapore: Springer Singapore
693 (Advances in Experimental Medicine and Biology), pp. 63–74. Available at:
694 https://doi.org/10.1007/978-981-15-3532-1_6.

695 Iwakoshi, N.N., Lee, A. and Glimcher, L.H. (2003) “The X-box binding protein-1
696 transcription factor is required for plasma cell differentiation and the unfolded protein
697 response,” *Immunological Reviews*, 194(1), pp. 29–38. Available at:
698 https://doi.org/10.1034/j.1600-065X.2003.00057.x.

699 Kitamura, D. *et al.* (1991) “A B cell-deficient mouse by targeted disruption of the
700 membrane exon of the immunoglobulin μ chain gene,” *Nature*, 350(6317), pp. 423–
701 426. Available at: https://doi.org/10.1038/350423a0.

702 Kräutler, N.J. *et al.* (2017) “Differentiation of germinal center B cells into plasma cells
703 is initiated by high-affinity antigen and completed by Tfh cells,” *Journal of*
704 *Experimental Medicine*, 214(5), pp. 1259–1267. Available at:
705 https://doi.org/10.1084/jem.20161533.

706 Lefranc, M.-P. (2011) “IMGT, the International ImMunoGeneTics Information
707 System,” *Cold Spring Harbor Protocols*, 2011(6), p. pdb.top115. Available at:
708 https://doi.org/10.1101/pdb.top115.

709 MacLean, A.J. *et al.* (2025) “Affinity maturation of antibody responses is mediated by
710 differential plasma cell proliferation,” *Science*, 387(6732), pp. 413–420. Available at:
711 https://doi.org/10.1126/science.adr6896.

712 Malladi, S.K. *et al.* (2025) “Germinal center–mediated broadening of B cell
713 responses to SARS-CoV-2 booster immunization,” *Science Immunology*, 10(112), p.
714 eadu4107. Available at: https://doi.org/10.1126/sciimmunol.adu4107.

715 McGuire, A.T. *et al.* (2014) “Antigen modification regulates competition of broad and
716 narrow neutralizing HIV antibodies,” *Science*, 346(6215), pp. 1380–1383. Available
717 at: https://doi.org/10.1126/science.1259206.

718 McGuire, A.T. *et al.* (2016) “Specifically modified Env immunogens activate B-cell
719 precursors of broadly neutralizing HIV-1 antibodies in transgenic mice,” *Nature*
720 *Communications*, 7(1), p. 10618. Available at: https://doi.org/10.1038/ncomms10618.

721 Merkenschlager, J. *et al.* (2023) “Continually recruited naïve T cells contribute to the
722 follicular helper and regulatory T cell pools in germinal centers,” *Nature*
723 *Communications*, 14(1), p. 6944. Available at: https://doi.org/10.1038/s41467-023-
724 41880-9.

Mesin, L. *et al.* (2019) “Restricted Clonality and Limited Germinal Center Reentry Characterize Memory B Cell Reactivation by Boosting,” *Cell*, 0(0). Available at: https://doi.org/10.1016/j.cell.2019.11.032.

Nussenzweig, M.C. *et al.* (1987) “Allelic Exclusion in Transgenic Mice That Express the Membrane form of Immunoglobulin μ,” *Science*, 236(4803), pp. 816–819. Available at: https://doi.org/10.1126/science.3107126.

Nussenzweig, M.C. *et al.* (1988) “A human immunoglobulin gene reduces the incidence of lymphomas in c-Myc-bearing transgenic mice,” *Nature*, 336(6198), pp. 446–450. Available at: https://doi.org/10.1038/336446a0.

Nutt, S.L. *et al.* (2015) “The generation of antibody-secreting plasma cells,” *Nature Reviews Immunology*, 15(3), pp. 160–171. Available at: https://doi.org/10.1038/nri3795.

Schaefer-Babajew, D. *et al.* (2023) “Antibody feedback regulates immune memory after SARS-CoV-2 mRNA vaccination,” *Nature*, 613(7945), pp. 735–742. Available at: https://doi.org/10.1038/s41586-022-05609-w.

Smith, T. (1909) “ACTIVE IMMUNITY PRODUCED BY SO CALLED BALANCED OR NEUTRAL MIXTURES OF DIPHTHERIA TOXIN AND ANTITOXIN,” *Journal of Experimental Medicine*, 11(2), pp. 241–256. Available at: https://doi.org/10.1084/jem.11.2.241.

Suan, D., Sundling, C. and Brink, R. (2017) “Plasma cell and memory B cell differentiation from the germinal center,” *Current Opinion in Immunology*, 45, pp. 97–102. Available at: https://doi.org/10.1016/j.coi.2017.03.006.

Tas, J.M.J. *et al.* (2016) “Visualizing Antibody Affinity Maturation in Germinal Centers,” *Science (New York, N.Y.)*, 351(6277), pp. 1048–1054. Available at: https://doi.org/10.1126/science.aad3439.

Todd, D.J. *et al.* (2009) “XBP1 governs late events in plasma cell differentiation and is not required for antigen-specific memory B cell development,” *Journal of Experimental Medicine*, 206(10), pp. 2151–2159. Available at: https://doi.org/10.1084/jem.20090738.

Viant, C. *et al.* (2020) “Antibody Affinity Shapes the Choice between Memory and Germinal Center B Cell Fates,” *Cell*, p. S0092867420313040. Available at: https://doi.org/10.1016/j.cell.2020.09.063.

Victora, G.D. and Nussenzweig, M.C. (2022) “Germinal Centers,” *Annual Review of Immunology*, 40(1), pp. 413–442. Available at: https://doi.org/10.1146/annurev-immunol-120419-022408.

Waisman, A. *et al.* (2007) “IgG1 B cell receptor signaling is inhibited by CD22 and promotes the development of B cells whose survival is less dependent on Igα/β,” *The Journal of Experimental Medicine*, 204(4), pp. 747–758. Available at: https://doi.org/10.1084/jem.20062024.

Wang, Y. *et al.* (2017) “Germinal-center development of memory B cells driven by IL-9 from follicular helper T cells,” *Nature Immunology*, 18(8), pp. 921–930. Available at: https://doi.org/10.1038/ni.3788.

Wang, Z. *et al.* (2023) “Memory B cell development elicited by mRNA booster vaccinations in the elderly,” *Journal of Experimental Medicine*, 220(9), p. e20230668. Available at: https://doi.org/10.1084/jem.20230668.

Woodruff, M.C. *et al.* (2018) “B Cell Competition for Restricted T Cell Help Suppresses Rare-Epitope Responses,” *Cell Reports*, 25(2), pp. 321-327.e3. Available at: https://doi.org/10.1016/j.celrep.2018.09.029.

Yan, Y. *et al.* (2025) “Antibody feedback establishes an affinity brake in the germinal center.” Immunology. Available at: https://doi.org/10.1101/2025.11.13.688298.

Zotos, D. and Tarlinton, D.M. (2012) “Determining germinal centre B cell fate,” *Trends in Immunology*, 33(6), pp. 281–288. Available at: https://doi.org/10.1016/j.it.2012.04.003.

Acknowledgements

We thank Kristie Gordon and Jean-Philip Truman for assistance with cell sorting, Thomas Eisenreich for help with mouse colony management and technical help; Masa Jankovic and Tacio A. Waldetario for laboratory support; and all members of the Nussenzweig laboratory and HIVRAD P01 (2P01AI100148) collaborators for helpful discussions.

Funding

This work was supported in part by by the Human Immunome Project and Michelson Medical Research Foundation's Michelson Prize: Next Generation Grant to D.S.B.; NIH grants 2P01AI100148-11 (HIVRAD) to M.C.N; UM1AI191237 (INSPIRE) to H.H. and M.C.N., 1UM1AI144462-01 (CHAVD) to M.C.N. and the Stavros Niarchos Foundation Institute for Global Infectious Disease Research. D.S.B. was supported in part by the National Center for Advancing Translational Sciences (NIH Clinical and Translational Science Award program, grant UL1-TR001866) and the Shapiro–Silverberg Fund for the Advancement of Translational Research. M.C.N. is a Howard Hughes Medical Institute investigators.

Author contributions

D.S.B., H.H. and M.C.N conceived the study. D.S.B and H.H. generated the novel mouse strains described in this manuscript. D.S.B., L.B. and H.H. designed and performed the experiments and interpreted data. G.S.S.S. performed bioinformatic analysis. C.R., L.D., M.A.E., D.G. and C.U. assisted and performed experiments. K.H.Y. assisted with mouse experiments and husbandry; B.H. and A.G. produced

recombinant proteins and antibodies. P.A. and L.S. provided HIV reagents. M.C.N. supervised the study, designed experiments and interpreted data. D.S.B., L.B., H.H. and M.C.N. wrote the manuscript. All authors edited the manuscript.

Competing interests

M.C.N. is on the scientific advisory board of Celldex Therapeutics. All other authors declare that they have no competing interests.

Data and materials availability

All data needed to evaluate the conclusions in the paper are available in the main text and supplementary materials. Reagents, including mouse strains, are available from H.H. and M.C.N. under a material transfer agreement with The Rockefeller University under reasonable request.

License information

This article is subject to HHMI's Open Access to Publications policy. HHMI lab heads have previously granted a nonexclusive CC BY 4.0 license to the public and a sublicensable license to HHMI in their research articles. Pursuant to those licenses, the Author Accepted Manuscript (AAM) of this article can be made freely available under a CC BY 4.0 license immediately upon publication.